Classification:
    Major category: Biological Sciences and Physical Sciences
    Minor category: Applied Physical Sciences and Medical Sciences

Title: Imaging Linear Birefringence and Dichroism in Cerebral Amyloid Pathologies

Authors: Lee-Way Jin[†], Kacey Claborn[#], Miki Kurimoto [#], Morten Geday[‡], Izumi Maezawa[†], Faranak Sohraby[†], Marcus Estrada [#], Werner Kaminksy[#], and Bart Kahr[#]

Department of Chemistry[#] and Department of Pathology[†], University of Washington, Seattle, Washington, USA, and Clarendon Laboratory[‡], Department of Physics, University of Oxford, Parks Road, Oxford, UK

Send Correspondence and Reprint Requests to:

Lee-Way Jin, M.D., Ph.D., Department of Pathology, Box 359791, University of Washington School of Medicine, Seattle, WA 98195-7470. Tel: 206-543-5088; FAX: 206-685-8356; Email: lwjin@u.washington.edu
Or
Dr. Bart Kahr, Ph.D., Department of Chemistry, Box 351700, University of Washington, Seattle, WA 98195-1700; Tel: 206-616-8195; FAX: 206-685-8665; Email: kahr@chem.washington.edu
Or
Dr. Werner Kaminsky, Ph.D., Department of Chemistry, Box 351700, University of Washington, Seattle, WA 98195-1700; Tel: 206-543-7585; FAX: 206-685-8665; Email: wernerka@u.washington.edu

Number of Text Pages: 11
Number of Figures: 4
Number of Tables: 0
Number of words in the abstract: 220
Number of characters in the paper: 35,595

Abbreviation: AD, Alzheimer's disease; CR, Congo red; LB, linear birefringence; LD, linear dichroism; CAA, cerebral amyloid angiopathy; Aβ, amyloid-β protein; GSS: Gerstmann-Sträussler-Scheinker disease; DS, Down syndrome.

Abstract

New advances in polarized light microscopy were employed to image Congo red stained cerebral amyloidosis in sharp relief. The rotating polarizer method was used to separate the optical effects of transmission, linear birefringence, extinction, linear dichroism, and orientation of the electric dipole transition moment, and to display them as false color maps. These effects are typically convolved in an ordinary polarized light microscope. In this way, we show for the first time that the amyloid deposits in Alzheimer's disease plaques contain structurally disordered centers, providing clues to possible mechanisms of crystallization of amyloid *in vivo*. Comparisons are made with plaques from tissues of subjects having Down syndrome and prion disease. In plaques characteristic of each disease, the Congo red molecules are radially oriented about the centers. The optical orientation in amyloid deposited in blood vessels from subjects having cerebral amyloid angiopathy was 90° out of phase from that in the plaques, suggesting that the fibrils run tangentially with respect to the circumference of the blood vessels. Our result supports an early model that Congo red molecules are aligned along the long fiber axis and is in contrast to the most recent binding models that are based upon computation. This investigation illustrates that the latest methods for the optical analysis of heterogeneous substances are useful for *in situ* study of amyloid.

Formatted

Formatted

2

Introduction

The abnormal transformation of proteins to amyloid fibrils is closely related to the so-called conformational diseases that include the common neurodegenerative disorders, such as Alzheimer's disease (AD) and prion diseases. The kinetic and structural bases of fibrillogenesis in these diseases are as yet undetermined. Nevertheless, the presence of amyloid in diseased tissues has been utilized for the purpose of pathological diagnosis and construction of theories of pathogenesis. A structural characterization and categorization of various forms of amyloid aid accurate diagnosis of amyloid disorders and further our mechanistic understanding of an increasing list of conformational diseases.

The principal diagnostic criterion of amyloidosis, established by Divry and Florkin (1), is the detection with a polarizing optical microscope of so-called "apple green" birefringence (2-6) from Congo red (CR) stained tissue sections (7). Despite the durability of this assay, the optical characterization of amyloid has not progressed and is ambiguous (8, 9). The birefringence is rarely quantified, a problem further confounded by the fact that CR does not stain amyloid consistently, and diagnosis by staining is dependent on the skill of the investigator. Clearly, new optical contrast mechanisms are required for simple, reliable amyloid diagnosis (10, 11).

Here we show that recent advances in polarized light microscopy can be used to quickly quantify and refine our description of CR stained amyloid. In particular, we have applied a newly developed imaging system to separate the optical transmission, refractive index anisotropy (linear birefringence, LB), and optical extinction that are otherwise convolved to produce the ill-defined apple green birefringence by conventional techniques. Moreover, we show that the system can be used to determine the absorption anisotropy (linear dichroism, LD) and the average orientation of the electric dipole transition moment. The resulting micrographs that rely on sensitive CCD intensity measurements provide polarized light images of Congophilic amyloid with greater structural resolution than previously reported. In this way, we have studied two forms of amyloid seen in the brains of AD subjects: amyloid in neuritic plaques, one of the hallmarks of Alzheimer pathology, and cerebral amyloid angiopathy (CAA). These two forms of amyloid, albeit in different anatomic structures, are both largely composed of amyloid-β protein (Aβ) species. For comparison, we have also studied amyloid seen in Gerstmann-Sträussler-Scheinker disease (GSS), composed principally of the transformed prion protein, as well as plaques seen in Down syndrome (DS), also composed of Aβ.

Materials and Methods
Tissue Preparation

All brain tissues used were obtained from the brain bank of the Alzheimer's Disease Research Center at the University of Washington, Seattle. The protocols used in this study were approved by the IRB of the University of Washington. The average postmortem interval for the tissues was ten hours. Five

to ten plaques from temporal cortex sections of the following subjects were analyzed for LB and LD anisotropy: sixteen cases of sporadic Alzheimer's disease (AD, age 71 to 92 years), all of them with cerebral amyloid angiopathy (CAA), five cases of Down syndrome (DS, age 45 to 68 years), and three cases of the telencephalic form of Gerstmann-Sträussler-Scheinker syndrome (GSS, age 32 to 38 years) with the A117V mutation of prion protein (12). Sections were typically obtained from mid-temporal gyrus. CR staining was performed by the method of Puchtler (13). Briefly, 10 μm formalin-fixed, paraffin-embedded sections were deparaffinized and hydrated to distilled water. Sections were then sequentially dipped in Meyer's hematoxylin for 3 min, alkaline sodium chloride for 20 min, and Congo red for 50 min, before dehydration with three changes of absolute alcohol and mounted.

Optical Imaging

Microscopy

The polarizing microscope, a prototype of the MetriPol System (http://www.metripol.com) now available from Oxford Cryosystems (Oxford, UK), was adapted with a stepper motor driven rotating polarizer, circular analyzer consisting of a linear analyzer and quarter wave plate aligned at 45°, an 8-bit monochrome CCD digital camera, and a PC with custom software able to deduce the absolute phase δ. The optical train, rotating polarizer-sample-circular analyzer, or rotating polarizer-sample, was used to image LB or LD, respectively. All measurements were made at 40x magnification. Three wavelengths, 547, 589, or 610 nm, were accessed with interference filters. The measurements were calibrated for a linear camera response, quarter wave plate alignment, and polarization bias of the light source, camera, and objective. Triplets of optical images associated with transmission, birefringence or dichroism, and optical orientation appear on the computer monitor within 15 seconds of centering the structure beneath the microscope objective. Image resolution is ~ 0.5% of the transmission, 0.2 nm of the retardance $L\Delta n$, 0.2 mm of the absorbance difference $L\Delta k$, and ~ 0.1° of the orientation (14).

Theory

The modified polarizing microscope is operated in two modes, where the full optical path (rotating polarizer-sample-circular analyzer) and reduced path (rotating polarizer-sample) are used to measure LB and LD, respectively. By modulating the intensity signal as a function of the polarizer angle α, the intensity ratio I/I_o (α) for each pixel is subject to a Fourier sum of the disparate optical contributions that are then displayed in false color images representing the overall transmission, the anisotropy (refraction (LB) and absorption (LD)), and the orientation (optical extinction (LB) and transition dipole moment (LD)). The expressions for transmitted intensity for the full and reduced paths are given in expressions (**a**) and (**b**) and are derived with Jones matrices (15).

(**a**)

$$\frac{I}{I_\circ} = \frac{1}{2}\left[1 + \sin^2(\boldsymbol{a} - \boldsymbol{j})\sin\boldsymbol{d}\right]$$

4

(b)

$$\frac{I}{I_\circ} = \cosh e + \sinh e \cos(2a - 2j\,')$$

Here, $d = 2pLDn/l$ (L is the thickness of the sample, Dn is the difference between the principle refractive indices or LB, λ is the wavelength of light) is the phase shift of the extraordinary and ordinary rays at the interface of the sample, j is the orientation of the slow vibration direction as measured counterclockwise from the horizontal axis. When using the reduced light path, f' is the orientation of the maximally absorbing axis as measured counterclockwise from the horizontal direction.

The LB is a function of the phase d by which the light waves propagating along the eigenmodes of the sample are offset. Similarly, the LD is measured in terms of the scaled differential transmission Dk along the eigenmodes of the sample, where $e = 2pLDk/l$ and $Dk = 2(T_{0^\circ} - T_{90^\circ})/(T_{0^\circ} + T_{90^\circ})$ ($T_{0^\circ,90^\circ}$ are the transmissions along the primary polarization directions). In this way, we precisely quantified LB and LD, creating an optical matrix of the diseased tissue.

Fourier analysis of the intensity data gives images of LB that are expressed as the absolute value of the sine of the phase difference ($|\sin d|$). Because $|\sin d|$ is a periodic function, the absolute value, or order, of d is not determined by this method. This 'order dilemma' was resolved by measuring the phase d at three close wavelengths and computing the derivatives of the resulting relative phases (16). The set of signs of the three derivatives unambiguously defines the absolute phase d and therefore the absolute birefringence.

Results

CR stains the core structure of two kinds of plaques distinguishable by Bielschowsky's silver stain. They are classical plaques consisting of an amyloid core and a corona, and compact plaques that are cores without coronas. Representative micrographs of tissue sections containing CR stained amyloid cores are shown in Figure 1 (A = AD, B = GSS, C = DS). Each plaque is red (λ_{max} = 515-538 nm) (17) in linearly polarized white light (I). Between crossed polarizers the apple-green birefringence is apparent (II). Figure 2 shows images of each pathologic structure in Figure 1, as well as an additional DS plaque indicated as D in Figure 2. The Fourier separation of the intensity signal as a function of polarizer rotation angle yields the anisotropies of refraction, $|\sin\delta|$ (I), and absorption, $\tanh\varepsilon$ (III), with the related orientations of the optical extinction position, f (II) and transition dipole moment, f' (IV).

AD plaque amyloid is unambiguously characterized by its affinity for CR (Figure 1/IA) and apple green birefringence (Figure 1/IIA), punctuated by a dark cross of extinction indicating a radially ordered spherical body (1, 18). These features are reiterated in the orientation images of LB (Figure 2/IIA) and LD (Figure 2/IVA). The colors that represent the angular orientation of the slowest

5

light vibration and most strongly absorbing direction, respectively, move smoothly around the black holes in the plaques, regions below which the birefringence and dichroism was vanishingly small. Perhaps the most striking feature of the MetriPol images (see Figures 2/IA through IVC) is the disordered center within the amyloid core, which is disguised by the extinction condition in Figure 1/II. These centers have an average diameter of 5 μm (range, 2-8 μm). In maps of transmission (not shown) these black holes clearly contain CR and presumably protein, but nevertheless anisotropy can not be detected.

The amyloid core in AD plaque in Figure 1 is compact and round, in the GSS plaque is stellated and larger, and in the DS plaque has a morphology and size that is somewhere in between. These morphological observations are consistent with those revealed by other microscopic methods (19, 20). While these general characteristics were most frequently representative of each disease, all three morphologies were observed sometimes in tissue samples from subjects having suffered from each of the three diseases. A subset of DS plaques shows an alternative amyloid morphology, broken rather than radial (Figure 2, column D). They were present in all 5 DS cases. Morphologically they appear similar to the "fibrous plaques" described in DS (20).

The ambiguity of the π periodicity inherent in the sinusoidal equation (**a**) governing LB was resolved using the order method previously described. All samples showed first order birefringence ($\delta < \pi/2$).

Figure 3 shows CR stained amyloid from the blood vessels of a subject burdened with CAA. Again the CR molecules are oriented radially, but there is a 90° phase shift as compared with the plaques. The phase shift is apparent when comparing the colors representing the optical orientation in Figure 2/II A-C as well as IV A-C (red is horizontal) with lower images in Figure 3 (red is vertical).

Discussion

Our *in situ* investigation of CR stained amyloid illustrates a new way to visualize and quantify birefringence. The images presented above are the most detailed and informative pictures of amyloid yet made with an optical microscope, revealing previously obscured structural features including disordered centers and well defined contours. Using the MetriPol method, we have demonstrated an absolute first order LB of amyloid deposits in tissues sections and the LD in the same tissue sections. Our results demonstrate with unprecedented precision the orientation of the slow axis of CR stained amyloid deposits and the orientation of the CR molecules with respect to the fibrils, a long debated issue. Our results also provide clues to the *in vivo* mechanism of amyloid formation. Significantly, in contrast to methods employed in many previous biophysical studies of amyloid, our method does not require isolation of fibrils from their tissue environment, the procedures of which potentially alter the structure of amyloid.

As well stated by Steensma: "At the dawn of the 21st century…the diagnostic test of choice for amyloidosis has not changed in decades…Congo red is still the 'king of dyes'." (21) Therefore, it may well be of value to bring the latest methods for the optical analysis of heterogeneous substances to bear on the characterization of CR stained amyloid. A standard procedure for staining

amyloid with CR was established by Puchtler *et al*. (12) who surmised that the dye was attached via unspecified hydrogen bonds and "ionic linkages". Lillie (22) invoked hydrogen bonding as the major mechanism of association as did Glenner *et al.* (23), Mera and Davies (24), and Turnell and Finch (25), but Glenner assigned equal importance to hydrophobic interactions, the principal non-covalent interaction according to Pigorsch *et al.* (26) while Mera and Davies invoked van der Waals forces, the principle non-covalent interaction according to Horobin (27). Turnell and Finch, leaving no stone unturned, cited the importance of hydrophobic and van der Waals interactions in addition to H-bonding. Ionic forces were specified by Klunk *et al.* (28) as well as Puchtler (29) who later favored "non-ionic" interactions, similarly preferred by Katenkamp and Stiller (30). Recent experiments were aimed as specifying more precisely the CR point(s) of attachment. Kirschner (31, 32) and coworkers identified histidine residues as the most "Congophilic". Cavillon *et al.* (33) preferred arginine while Li *et al.* (34) liked lysines (as well as hydrophobic interactions). It is safe to conclude that the process of amyloid staining by CR is not fully understood.

Irrespective of the staining mechanism, simple inspection with a polarizing microscope can nevertheless provide information about the orientation of the dyes within amyloid plaques. However, there does not seem to be a consensus as to whether the transition dipole moments of the CR molecules are parallel (30, 35, 36) or perpendicular (34, 37, 38) to the fiber axes. Clearly, new methods for the optical analysis of CR stained amyloid would be desirable in order to identify the dyeing mechanism. The f and f' images in Figures 2 and 3 clearly show the radial orientation of anisotropic structures. Furthermore, their relationship suggests a solution to this fundamental question regarding the mechanism of staining of amyloid.

It is known that the amyloid fibrils in AD plaques form radial aggregates, and that the transition moment in CR runs along the long molecular axis (39). Therefore, the CR molecules are aligned along the long fiber axis as required by the fact that the fibrils lying on the horizontal axis have values of f and f' of ~ 0° in Figure 2/II and IV. In CAA there is a 90°-phase shift. Assuming that the molecular mechanism of CR staining is the same in both CAA and amyloid plaques, this indicates that the fibrils run around the blood vessels. A summary of our view of CR orientation in plaques and blood vessels is shown in Figure 4. Our judgments in this regard merely confirm what the earliest polarized light microscopists proposed, however, this judgement has been curiously disregarded in recent years.

A recent contribution to the debate on CR orientation comes from Carter and Chou (40) who built an atomic model of CR bound to amyloid by analogy with a published crystal structure of CR bound to insulin (25). In this model, CR is interleaved between the two strands of the amyloid β−sheet. Other model builders have supported the view of orthogonal CR and amyloid fibril long axes (41). This picture can no longer be supported in light of the MetriPol images that make the dichroism and the orientation of the transition moment strikingly apparent.

7

The anisotropy maps (Figure 2/I&III) demonstrate the disordered centers of amyloid cores, despite that these centers incorporated CR. This finding is reminiscent of the thioflavin S-positive and non-Aβ-immunoreactive centers of AD amyloid cores described by Schmidt et al (20). However, the structurally defined centers observed here may not exactly correspond to the reported cytochemically defined centers. First, the former are in average smaller than the latter. Second, the former are equally observed in DS amyloid, while the latter are not. In any event, our findings of the sharp change in the order of the medium undoubtedly holds clues to the biopathological crystallization mechanism of amyloid. Are the fibrils organizing around a catalytic, disordered core, or is the mass crystallizing from the outside in, like a geode? An answer to this question has significant implications. Amyloid formation is considered to be a nucleation-dependent process analogous to the seeding of a crystal (42). However, the molecular composition of the "nucleus" and its seeding mechanism in amyloid formation is not understood. *In vitro* and *in vivo* evidence has suggested that amyloid formation can be seeded by a preformed fibril (11, 42). Assuming the fibrils grow around the disordered center, then the center may be composed of preformed fibrils (with affinity to CR, but not yet organized to give detectable anisotropy) as seeds for amyloid crystallization, and may be composed of additional molecules that have been shown to promote amyloid formation, such as cholesterol, fatty acids, or proteoglycan. Alternatively, if the fibrils grow from the outside in, the disordered center may represent the partially structured intermediates undergoing active organization, catalyzed by surrounding structured fibrils. Our results point out the necessity of analyzing the molecular composition of the disordered centers, in order to understand the nature of either the catalytic center or the transforming intermediates that are instrumental in the development of structured fibrils.

Comparable methods of orientation independent imaging have been developed. These include the PolScope (43), as well as differential polarized light microscopies developed by Bustamante and coworkers (44), Tower and Tranquillo (45), Poenie and coworkers (46), and Ho and coworkers (47). These techniques, should in principle provide a similar view of CR stained amyloid.

In a very forward thinking paper, Benditt and coworkers (17) realized that a complete characterization of CR stained amyloid would ultimately include optical rotary dispersion and circular dichroism. New microscopes are currently being developed in our laboratories in order to image chiroptical effects in ordered media.

Acknowledgements

References

1. Divry, P. & Florkin, M. (1927) *C R Soc Biol* **97**, 1808-1810.
2. Missmahl, H. P. & Hartwig, M. (1952) *Virchow's Arch Pathol Anat Physiol* **324**, 489-508.
3. Cohen, A. S. (1967) *New Engl J Med* **277**, 522-530.
4. Elghetany, M. T. & Saleem, A. (1988) *Stain Technol* **63**, 201-212.
5. Sipe, J. D. & Cohen, A. S. (2000) *J Struct Biol* **130**, 88-98.
6. Rosenblum, W. I (2002) *Neurobiol Aging* **23**, 225-230.
7. Bennhold, H. (1922) *Münchener Medizinische Wochenschrift* **69**, 1537-1538.
8. Hawkins, P. N., Lavender, J. P., & Pepys, B. (1990) *N Engl J Med* **324**, 508-513.
9. Linke, R. P., Gärtner, H. V., & Michels, H. (1995) *J Histochem Cytochem* **9**, 863-869.
10. Wolman, M. & Bubis, J. J. (1965) *Histochemie* **4**, 351-356.
11. Kisilevsky, R. (2000) *J Struct Biol* **130**, 99-108.
12. Nochlin, D., Sumi, S. M., Bird, T. D., Snow, A. D., Leventhal, C. M., Beyreuther, K., & Masters, C. L. (1989) *Neurology* **39**, 910-918.
13. Puchtler, H., Sweat, F., & Levine, M. (1962) *J Histochem Cytochem* **10**, 355-364.
14. Glazer, A. M., Lewis, J. G., & Kaminsky, W. (1996) *Proc R Soc London A* **425**, 2751-2765.
15. Jones, R. C. (1941) *J Opt Soc Am* **31**, 488-503.
16. Geday, M. A., Kaminsky, W., Lewis, J. G., & Glazer, A. M. (2000) *J Microsc* **198**, 1-9.
17. Taylor, D. L., Allen, R. D., & Benditt, E. P. (1974) *J Histochem Cytochem* **22**, 1105-1112.
18. Kelényi, G. (1967) *Acta Neuropathol* **7**, 336-348.
19. Allsop, D., Kidd, M., Landon, M., & Tomlinson, A. (1986) *J Neurol Neurosurg Psychiatry* **49**, 886-892.
20. Schmidt, M. L., Robinson, K. A., Lee, V. M., & Trojanowski, J. Q. (1995) *Am J Pathol* **147**, 503-515.
21. Steensma, D. P. (2001) *Arch Pathol Lab Med* **125**, 250-252.
22. Lillie, R. D. (1977) in *H. J. Conn's biological stains*, 9th ed., (The Williams & Wilkins Co., Baltimore), pp. 147–148.
23. Glenner, G. G., Eanes, E. D., Bladen, H. A., Linke, R. P., & Termine, J. D. (1974) *J Histochem Cytochem* **22**, 1141-1158.
24. Mera, S. L. & Davies, J. D. (1983) *J Path* **141**, 547-547.
25. Turnell, W. G. & Finch, J. T. (1992) *J Mol Biol* **227**, 1205-1223.
26. Pigorsch, E., Elhaddaoui, A., & Turrell, S. (1994) *Spectromchim Acta* **50A**, 2145-2152.
27. Horobin, R. W. (1980) *J Microsc* **119**, 345-355.
28. Klunk, W. E., Pettegrew, J. W., & Abraham, D. J. (1989) *J Histochem Cytochem* **37**, 1273-1281.
29. Puchtler, H., Waldrop, F. S., & Meloan, S. N. (1985) *Appl Pathol* **3**, 5-17.
30. Katenkamp, D. & Stiller, D. (1972) *Histochemie* **29**, 37-43.

31. Kirschner, D. A., Inouye, H., Duffy, L. K., Sinclair, A., Lind, M., & Selkoe, D. J. (1987) *Proc Natl Acad Sci USA* **84**, 6953-6957.
32. Inouye, H., Nguyen, J. T., Fraser, P. E., Shinchuk, L. M., Packard, A. B., & Kirschner, D. A. (2000) *Amyloid* **7**, 179-188.
33. Cavillon, F., Elhaddaoui, A., Alix, A. J. P., Turrell, S., & Dauchez, M. (1997) *J Mol Struct* **408-409**, 185-189.
34. Li, L., Darden, T. A., Bartolotti, L., Kominos, D., Pedersen, L. G. (1999) *Biophys J* **76**, 2871-2878.
35. Wolman, M. & Bubis, J. J. (1965) *Histochemie* **4**, 351-356.
36. Glenner, G. G. & Page, D. L. (1976) *Int Rev Exp Pathol* **15**, 1-92.
37. Cooper, J. H. (1974) *Lab Invest* **31**, 232-238.
38. Elhaddaoui, A., Pigorsch, E., Delacourte, A., & Turrell, S. (1995) *J Mol Struct* **347**, 363-369.
39. Gueft, B. & Ghidoni, J. J. (1963) *Am J Path* **43**, 837-854.
40. Carter, D. B. & Chou, K-C. (1998) *Neurobiology Aging* **19**, 37-40.
41. George, A. R. & Howlett, D. R. (1999) *Biopolymers* **50**, 733-741.
42. Harper, J. D. & Lansbury, P. T. Jr. (1997) *Annu Rev Biochem* **66**, 385-407.
43. Oldenbourg, R. & Mei, G. (1995) *J Microsc* **180**, 140-147.
44. Bustamante, C., Kim, M., & Beach, D. A. (1988) *Polarization Spectroscopy of Ordered Systems* **242**, 313-356.
45. Tower, T. T. & Tranquillo, R. T. (2001) *Biophys J* **81**, 2954-2963.
46. Kuhn, J. R., Wu, Z., & Poenie, M. (2001) *Biophys J* **80**, 972-985.
47. Newton, R. H., Haffegee, J. P., & Ho, M. W. (1995) *J Microsc* **180**, 127-130.

Figure Legends

Figure 1. CR stained amyloid plaques characteristic of three diseases: (A) AD; (B) GSS, and (C) DS. I: amyloid in linearly polarized white light, II: amyloid between crossed polarizers showing apple-green birefringence.

Figure 2. Optical images of CR stained plaques characteristic of: (A) AD, (B) GSS, and (C,D) DS. I: |sin$d$| = the absolute value of the sine of the phase difference where $d = 2\pi\Delta nL/l$. II: f = the optical extinction angle in degrees as measured counterclockwise from the horizontal axis. I and II are measured off-resonance at 610 nm. III: hyperbolic tangent of the extinction where $e = 2pLDk/l$ and $Dk = 2(T_{0°} - T_{90°})/(T_{0°} + T_{90°})/(T_{0°,90°})$. IV. f = angle in degrees from the most absorptive direction as measured counterclockwise from the horizontal axis. . III and IV are measured on-resonance at 5547 nm. Scales for |sinδ| and tanhϵ are not indicated in the legends and are given here: I.A. 0.07-0.23; I.B. 0.07-0.28; I.C. 0.05-0.24; I.D. 0.05-0.18; III.A. 0.05-0.25; III.B. 0.06-0.46; III.C. 0.04-0.29; III.D. 0.04-0.16. Pixels with values below the minimum specified here were set to black. In the centers of the plaques sin$d$ and tanh$e$ were ~ 0.02.

Figure 3. Optical images of CR stained amyloid associated with a blood vessel from a subject burdend with CAA. A (top): |sinδ|, A (bottom): f, B (top): tanh ϵ, B (bottom) f.

Figure 4. Cartoon showing fibril and CR orientations in plaques (A) and blood vessels (B). The state of amyloid in the disorder center in (A) is not represented, as it is unresolved.
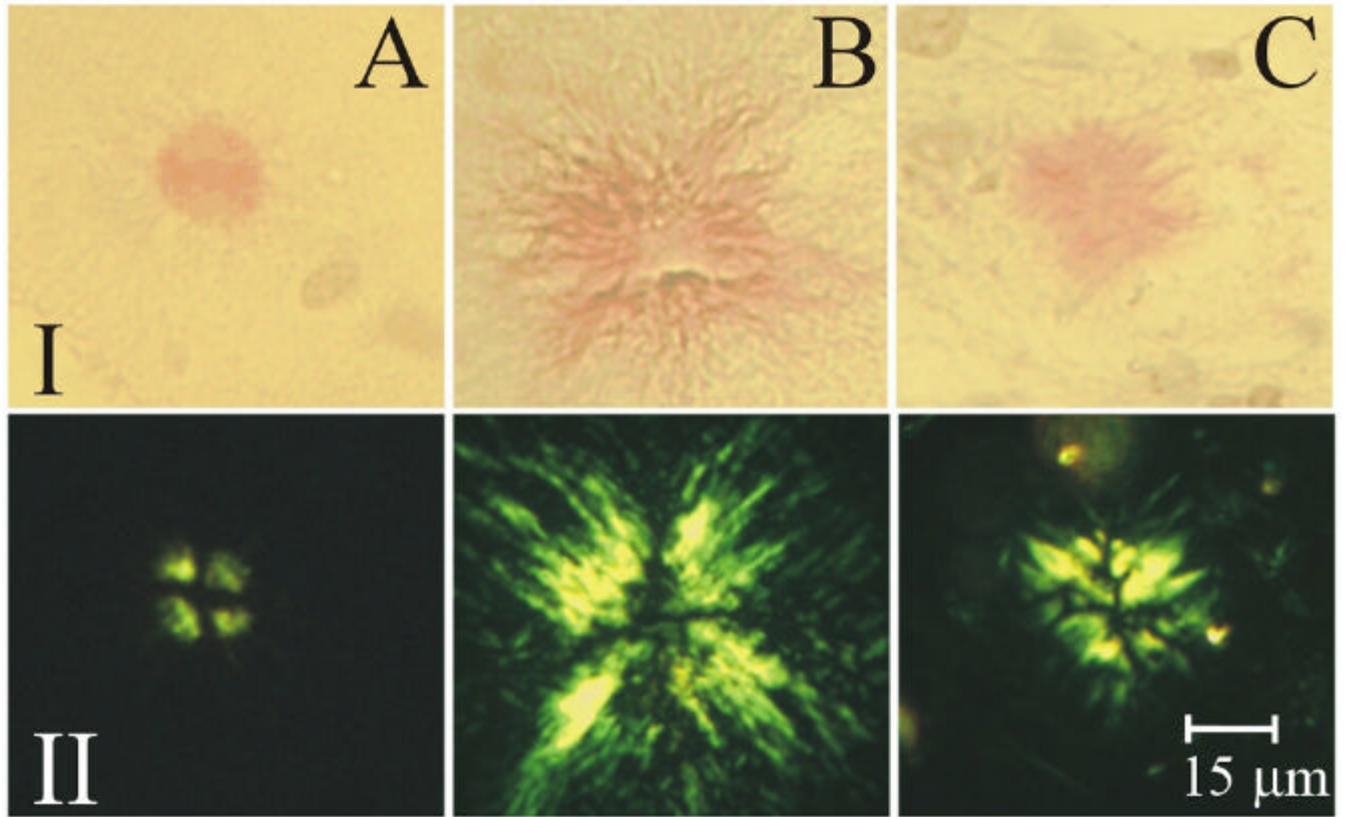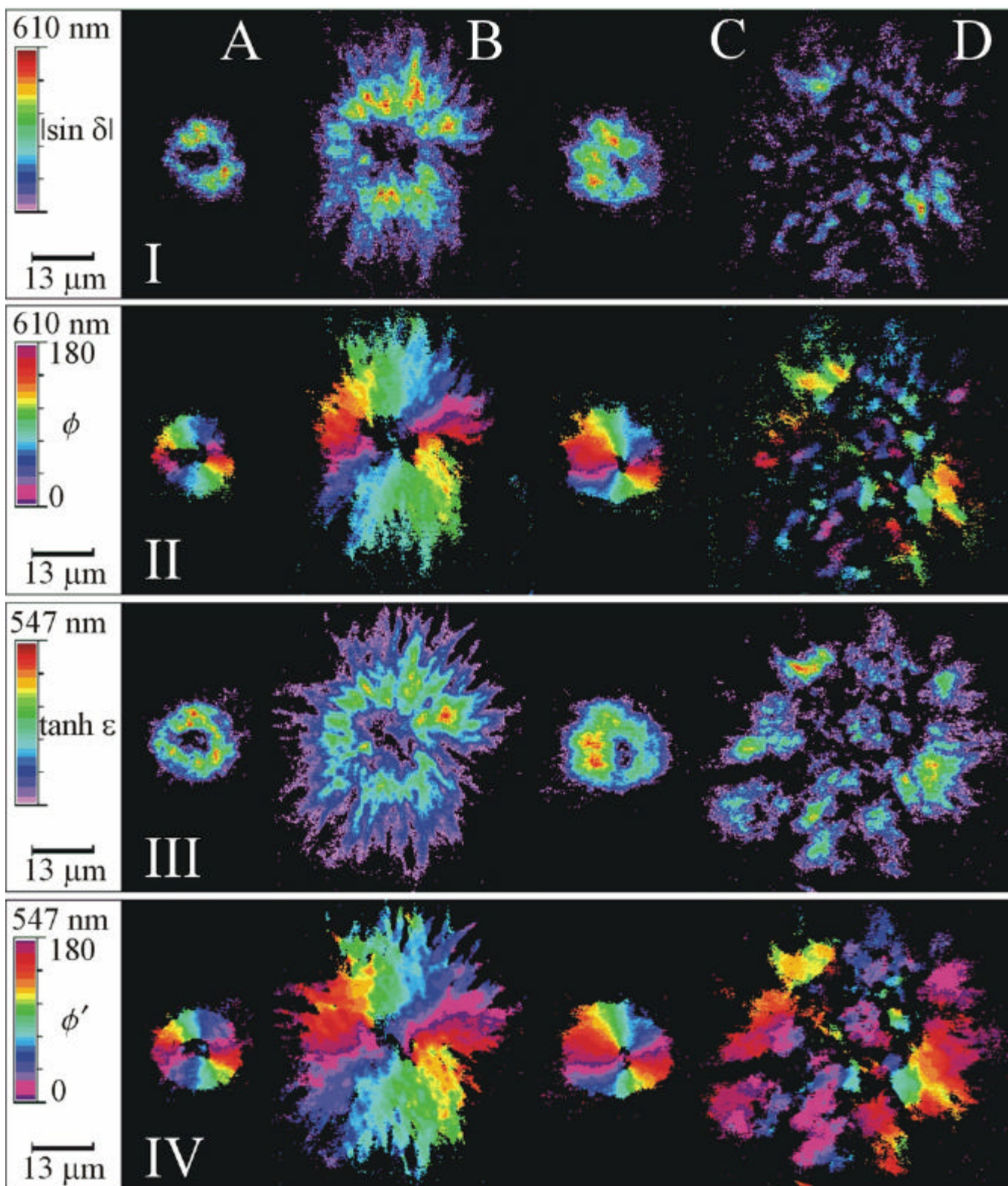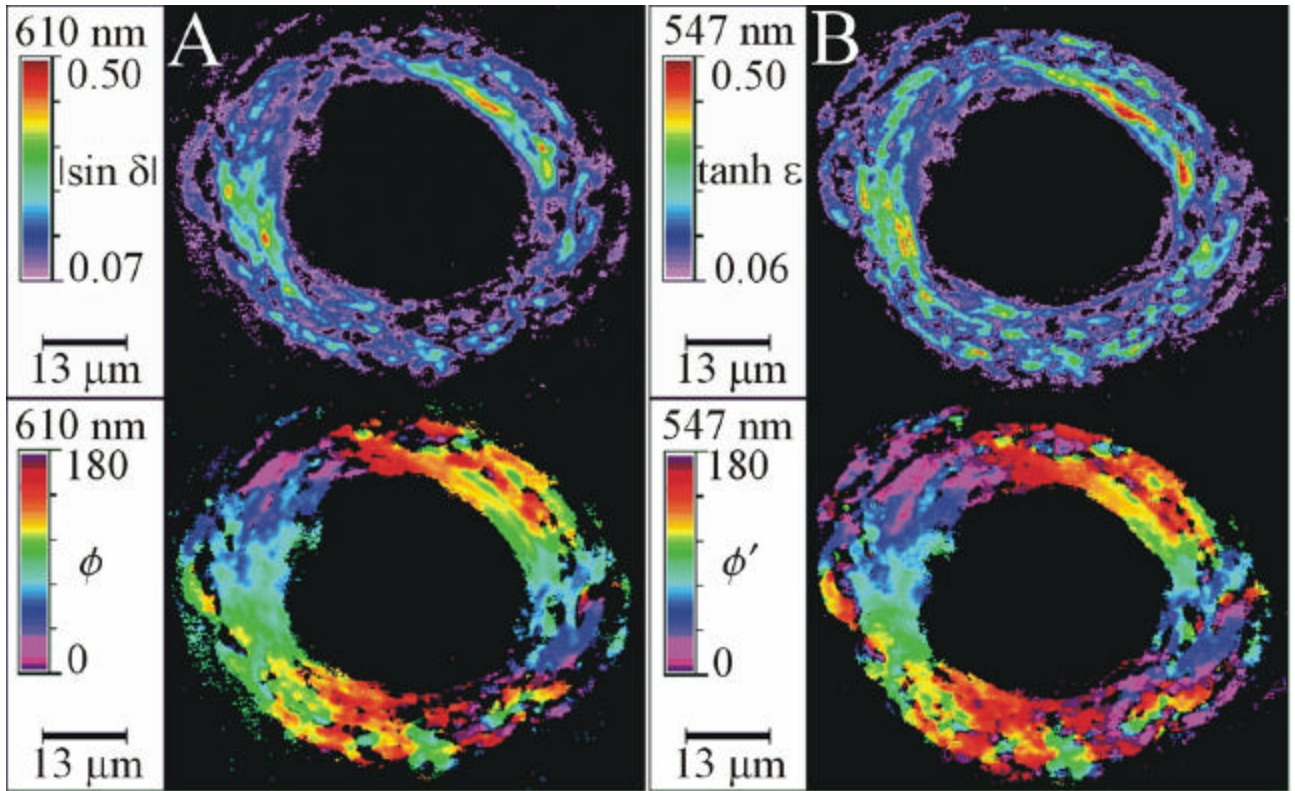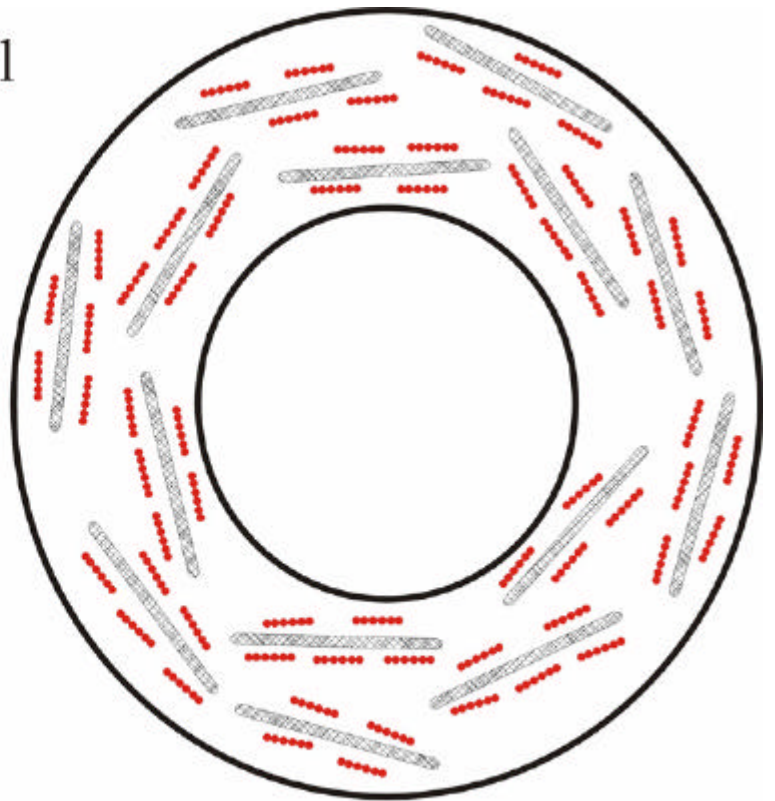
Figure 1

Figure 2

Figure 3

Figure 4